Microscopic interplay of temperature and disorder of a 1D elastic interface

Nirvana Caballero,[1,*] Thierry Giamarchi,[1] Vivien Lecomte,[2] and Elisabeth Agoritsas[3]

[1] *Department of Quantum Matter Physics, University of Geneva, 24 Quai Ernest-Ansermet, CH-1211 Geneva, Switzerland*

[2] *Université Grenoble Alpes, CNRS, LIPhy, FR-38000 Grenoble, France*

[3] *Institute of Physics, Ecole Polytechnique Fédérale de Lausanne (EPFL), CH-1015 Lausanne, Switzerland*

(Dated: November 17, 2021)

We compute numerically the roughness of a one-dimensional elastic interface subjected to both thermal fluctuations and a quenched disorder with a finite correlation length. We evidence the existence of a novel power-law regime, at short lengthscales, resulting from the microscopic interplay between thermal fluctuations and disorder. We determine the corresponding exponent $\zeta_{\rm dis}$ and find compelling numerical evidence that, contrarily to available (variational or perturbative) analytic predictions, one has $\zeta_{\rm dis} < 1$. We discuss the consequences on the temperature dependence of the roughness and the connection with the asymptotic random-manifold regime at large lengthscales. We also discuss the implications of our findings for other systems such as the Kardar-Parisi-Zhang equation.

Interfaces are ubiquitous in nature and provide remarkable challenges both from the theoretical and experimental fronts [1]. Experimentally they span very different underlying physics and characteristic scales, with examples ranging *e.g.* from domain walls in ferromagnetic or ferroelectric thin films [2–9] to imbibition fronts in porous media [10], fracture surfaces [11–13] and growing fronts of cell colonies [14–16]. On the theory side, describing the competition between the elastic interactions that tend to order them, and the temperature and system heterogeneity that hinder this tendency, is a considerable theoretical challenge, with a resulting out-of-equilibrium physics akin to the one of glasses [17].

A successful theoretical tool to study interfaces is provided by the *disordered elastic systems* framework [18–23]: interfaces are modeled as elastic objects evolving in a quenched disordered landscape and subject to thermal noise. Remarkably, this minimal description is enough to account for many key statistical features of the geometry and dynamics of both static or driven interfaces [24]. In particular, geometrical fluctuations are known to be scale-invariant at sufficiently large lengthscales, evidenced by a power-law behavior of the so-called roughness: the variance of the relative displacement of the interface between two points separated by a given distance. The associated roughness exponent provides a robust signature of the universality class to which an interface belongs [25], depending solely on its dimensionality and on the nature of both its elasticity and underlying disorder [22].

However, beyond this hallmark of universality, the roughness prefactor itself encodes quantitative information about the microphysics of a given system. Labelled as non-universal, this roughness feature has been poorly exploited up to now, despite of its crucial experimental relevance for the quantitative determination of characteristic scales and the validity range of theoretical predictions in a given experimental setup [26–28]. At equilibrium its amplitude is fixed once and for all at short lengthscales by the microscopic interplay between thermal fluctuations and a spatially-correlated disorder. The resulting temperature crossover below a characteristic energy scale $T_c(\xi)$, associated to the disorder strength and finite correlation length ξ, is thus a macroscopic 'smoking gun' of the spatial structure of microscopic disorder [29–31]. Furthermore, analytical studies using perturbative [32] or variational [29] methods suggest at short-lengthscales a power-law excess roughness –in addition to thermal fluctuations– with a characteristic exponent $\zeta_{\rm dis} = 1$. Unfortunately a quantitative characterization of this microscopic interplay, usually hidden below experimental resolution, has been difficult to access up to now.

For static one-dimensional (1D) interfaces, understanding this interplay is also important to characterize both the finite-time and steady-state fluctuations of the celebrated 1D Kardar-Parisi-Zhang (KPZ) equation [33, 34]. Considerable advances were achieved recently on that front [35–39] allowing for the computation of universal exponents and distributions [38, 39], but mainly for spatially-uncorrelated noises. Nevertheless, a regime which still resists an exact analytical treatment is the low-temperature limit in a spatially-correlated disorder [30, 31, 40–46], despite of its high relevance to analyze experimental realizations of KPZ [38, 47–49], or of Burgers turbulence [50, 51] under a large-scale forcing.

In this paper, we address these issues by numerically computing the roughness of an interface with both correlated disorder and thermal fluctuations. We unveil the key regime where the interplay between temperature and disorder leads to an excess of roughness – compared to bare thermal fluctuations – and show that it relaxes towards a power-law behavior $B_{\rm dis}(r) \approx A_{\rm dis}(T)\, r^{2\zeta_{\rm dis}}$ at short lengthscale r. Previous analytical but approximate predictions propose $\zeta_{\rm dis} = 1$; yet, we show compelling numerical evidence that $\zeta_{\rm dis} < 1$, which has important consequences on the temperature dependence of the roughness and the connection to the asymptotic

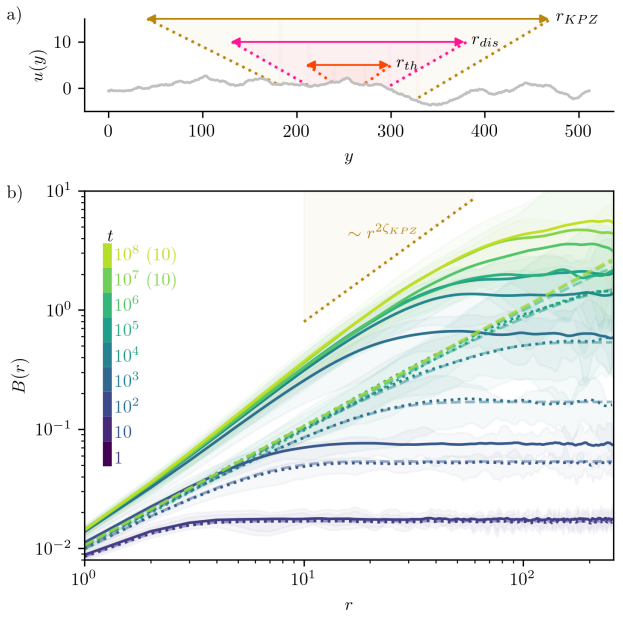

Figure 1. a) Snapshot of an initially flat interface described by the field $u(y,t)$, after having evolved under the qEW dynamics (1) up to a time $t = 10^9$. b) Roughness $B(r,t)$ obtained for interfaces that evolved during different times (indicated by the color scale) averaged over 50 realizations (or 10 realizations for the larger studied times -indicated in the color scale-) with and without disorder (continuous and dotted lines, respectively) at T=0.01 and $\epsilon = 0.1$. Shaded fluctuations are shown with the same color scale. Dashed lines correspond to the analytical prediction (4) for the roughness evolution in a clean system. The expected power-law at large distances in the random-bond disordered case ($\sim r^{\zeta_{\rm KPZ}}$ with $\zeta_{\rm KPZ} = 2/3$) is indicated in a brown dotted line at the top.

random-manifold regime.

We consider a 1D interface parametrized at time t by $(y, u(y,t)) \in [0, L] \times \mathbb{R} \subset \mathbb{R}^2$, as shown in Fig. 1 a). The displacement field $u(y,t)$ is univalued with periodic boundary conditions $u(y = 0, t) = u(y = L, t)$. Starting from a flat initial condition $u(y, t = 0) = 0$ we let the interface evolve according to the so-called quenched Edwards–Wilkinson (qEW) equation [52–55] in the absence of an external force:

$$\eta \partial_t u(y,t) = c\partial_y^2 u(y,t) + F_p\left(y, u(y,t)\right) + \xi(y,t)\,. \quad (1)$$

Thermal fluctuations are described by a Gaussian white noise $\xi(y,t)$ of zero mean and two-point correlator $\langle \xi(y_1,t_1)\xi(y_2,t_2)\rangle = 2\eta T\delta(y_2 - y_1)\delta(t_2 - t_1)$, where $\langle \ldots \rangle$ denotes the thermal average, η is an effective friction coefficient and T is the temperature (the Boltzmann constant is fixed to $k_B = 1$). We fix the units of time and energy, respectively, by setting $\eta = 1$ and the elastic constant $c = 1$. The disorder is modeled through a quenched random potential $V_p(y,u)$ and its associated pinning force $F_p(y,u) = -\partial_u V_p(y,u)$, both Gaussian with zero mean and correlators:

$$\begin{aligned} \overline{V_p(y_1,u_1)V_p(y_2,u_2)} &= D\, R_\xi(u_2 - u_1)\,\delta(y_2 - y_1)\,, \\ \overline{F_p(y_1,u_1)F_p(y_2,u_2)} &= \Delta_\xi(u_2 - u_1)\,\delta(y_2 - y_1)\,, \end{aligned} \quad (2)$$

where $\overline{\cdots}$ denotes the average over disorder realizations. We consider the case of 'random-bond' disorder with finite correlation length ξ, *i.e.* with a short-range correlator $R_\xi(u) = \xi^{-1} R_1(u/\xi)$ normalized as $\int_{\mathbb{R}} {\rm d}u\, R_\xi(u) = 1$ and D the disorder strength. Both correlators are even and related through $\Delta_\xi(u) = -D\, R''_\xi(u)$ [21], so that $\int_{\mathbb{R}} {\rm d}u\, \Delta_\xi(u) = 0$.

We numerically integrate (1) with the Euler method and a time step $\Delta t = 10^{-2}$, keeping u as a continuous variable while discretizing the y direction in $L = 512$ segments of unit length. This qEW settings allow us to advantageously replace the Dirac $\delta(y - y')$ by the Kronecker $\delta_{yy'}$ in (2) and thus to implement an uncorrelated disorder along the internal direction y. In the transverse direction, the disorder potential is dynamically generated [55, 56] with random numbers taken from a uniform distribution in the range $[-\frac{\epsilon}{2}, \frac{\epsilon}{2}]$ at equidistant positions, spaced by $\Delta u = 1$. To obtain the random-bond pinning force at a particular point u we interpolate the two nearest random numbers with a linear spline and take its derivative with respect to u. With these settings the correlator $\Delta_\xi(u = u_2 - u_1)$ is given by a piecewise function, see Supporting Material (SM). Our effective parameters are then $\{\xi = 1, D = \frac{\epsilon^2}{12}\}$, where we took $\epsilon = 0.1$, and we explore $T \in \{0.005, \ldots, 0.074\}$ (see SM).

To characterize the geometrical fluctuations of the interface, we focus on the roughness function

$$B\left(r = |y_2 - y_1|, t\right) = \overline{\langle [u(y_2,t) - u(y_1,t)]^2 \rangle}\,. \quad (3)$$

It quantifies the variance of the relative displacements of the interface, as a function of the lengthscale r, and inherits the translation invariance in y of the microscopic disorder. For a clean system ($F_p(y) = 0$), we can compute analytically the full time dependence of this correlation for an infinite interface [52, 57]:

$$B_{\rm th}(r,t) = \frac{Tr}{c}\left[1 - \frac{1}{\sqrt{\pi} z r}\left(e^{-z^2 r^2} - 1\right) - \frac{2}{\sqrt{\pi}}\int_0^{zr} {\rm d}t\, e^{-t^2}\right] \quad (4)$$

where $z = \sqrt{\frac{\eta}{8ct}}$. At large times, (4) converges to the static thermal roughness $B_{\rm th}(r) \equiv \frac{Tr}{c}$. To disentangle the different contributions on the roughness function we introduce the excess roughness $B_{\rm dis} = B - B_{\rm th}$, defined as the difference between the total roughness and its analytical prediction in the clean case.

In Fig. 1, we show the time evolution of the roughness at a fixed temperature $T = 0.01$, averaged over several realizations, in either clean or disordered systems (with the same numerical seed for the thermal noise). For the clean case, the roughness is very well

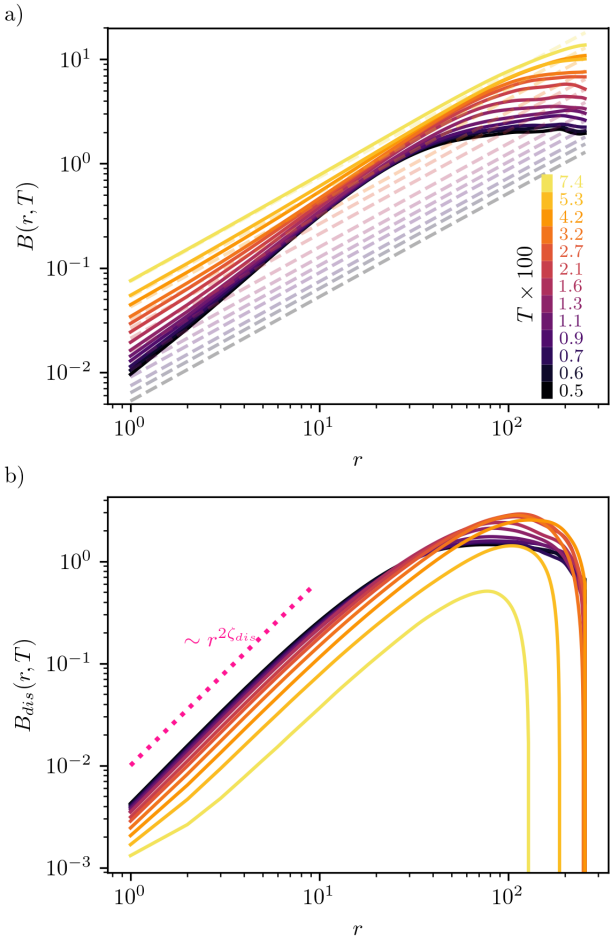

Figure 2. a) Roughness of interfaces evolving in a spatially-correlated disorder, for temperatures T ranging from 0.005 to 0.07. Each curve corresponds to an average over 50 realizations with increased statistics (see text) that evolved with the qEW dynamics (1) for a time $t = 10^6$ starting from a flat initial condition. Dashed lines indicate the analytical prediction for the roughness in the absence of disorder given by (4) at same $t = 10^6$. b) Corresponding excess roughness $B_{\rm dis}$ due to disorder, obtained as the difference between the total roughness and the analytical prediction (4) of the thermal roughness. The roughness decrease beyond $r = L/2$ is an artifact of the periodic boundary conditions. Our numerical study shows unambiguously the existence of a key power-law regime for the excess roughness existing at small scales and characterized by an exponent $\zeta_{\rm dis}$ different from the thermal and random manifold ones.

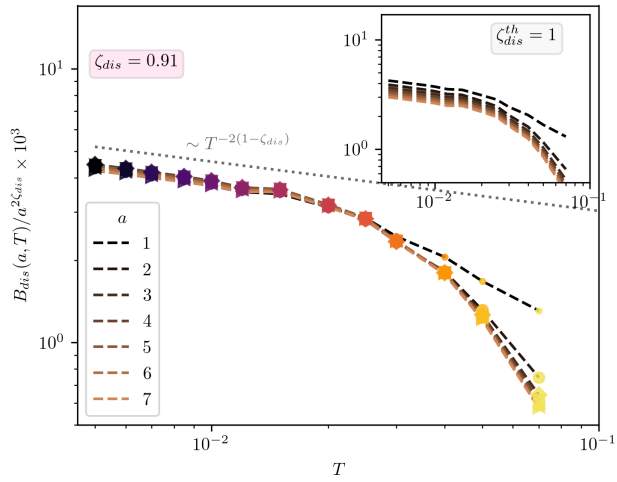

Figure 3. Collapse of the excess roughness $B_{\rm dis}(a,T)$ for different fixed lengthscales a as a function of temperature. The collapse is obtained with a power-law $a^{2\zeta_{\rm dis}}$, with $\zeta_{\rm dis} = 0.91 \pm 0.01$. The insert shows that if we force the use of $\zeta^{\rm th}_{\rm dis} = 1$ the collapse is lost – showing the sensitivity of our method to determine the exponent.

described by the analytical prediction (4). For the disordered case, at very large times and large lengthscales, the power-law $\sim r^{2\zeta_{\rm KPZ}}$ with $\zeta_{\rm KPZ} = \frac{2}{3}$, characteristic of a random-bond disorder, is reached. Note, however, that already after $t = 10^3$ the roughness has converged at short lengthscales ($r \lesssim 20$).

In Fig. 2 a) we show the total roughness function $B(r,T)$ at fixed large time $t = 10^6$ averaged over 50 realizations. To increase the statistics, for each realization that evolved for a time 10^6 we included 100 more configurations equally spaced in time intervals of 10^3. Note that this procedure allows us to considerably increase the statistics for lengthscales at which the interface has already equilibrated. In Fig. 2 b), we report the corresponding excess roughness $B_{\rm dis}(r,T)$ at different temperatures. The numerical data shows clearly the existence of a power-law regime of the roughness characterized by an exponent $\zeta_{\rm dis}$. This regime, which can be obscured by the existence of the large thermal component of the roughness depending on parameters, is nevertheless present and universal, and results from the interplay between the finite correlation of the disorder and the thermal fluctuations. As we will discuss below, besides the existence of the regime itself, the precise value of the exponent $\zeta_{\rm dis}$ has important consequences for the temperature dependence of the roughness.

A fitting of $B_{\rm dis}(r)$ with a power law $\sim r^{2\zeta_{\rm dis}}$ in the regime of small values of r gives an exponent $\zeta_{\rm dis} = 0.91$ with a temperature-dependent amplitude but given the importance of estimating whether $\zeta_{\rm dis} = 1$ or not, we explore below this issue in more details.

This result is further detailed in Fig. 3 where the rescaling of $B_{\rm dis}$ with this power-law $r^{2\zeta_{\rm dis}}$ is shown. The collapse of the curves is very sensitive to the precise value of the exponent and allows us to rule out with a high confidence a value of $\zeta_{\rm dis} = 1$ (see SM). Interestingly, the only currently available analytical predictions give a theoretical value $\zeta_{\rm dis} = \zeta^{\rm th}_{\rm dis} \equiv 1$: a finite-temperature perturbative approach [32] [58] and two different computations of $B(r)$ based on a

Gaussian-Variational-Method (GVM) scheme [29] [59]. Our numerical findings thus provide evidence that non-perturbative approaches are required to determine the exponent $\zeta_{\rm dis}$, and beyond the usual variational alternatives. Also, we checked that a different disorder distribution leads to the same value of $\zeta_{\rm dis}$ (see SM), supporting the robustness of $\zeta_{\rm dis} < 1$.

To analyze the implications of this result, we now determine the relevant lengthscales, first recalling previously known results. The static roughness $B(r) = B_{\rm th}(r) + B_{\rm dis}(r)$ crosses over from a thermal regime $B(r) \approx B_{\rm th}(r) = Tr^{2\zeta_{\rm th}}/c$ at very short lengthscales, to the random-manifold regime $B(r) \approx B_{\rm dis}(r) \approx \xi_{\rm eff}^2 (r/L_c)^{2\zeta_{\rm KPZ}}$ at lengthscales larger than a characteristic length L_c, closely related to the so-called 'Larkin length' in higher-dimensional interfaces [19, 60]. In our system, $\zeta_{\rm th} = \frac{1}{2}$ and $\zeta_{\rm KPZ} = \frac{2}{3}$. Previous analytical studies [29, 30, 44] have shown that $L_c = \frac{(T/f)^5}{cD^2}$ and $\xi_{\rm eff} = \frac{(T/f)^3}{cD}$, with a temperature-dependent parameter f. Defining the energy scale $T_c = (\xi c D)^{1/3}$, we expect a monotonous crossover from $f \approx 1$ at $T \gg T_c$ to $f \sim T/T_c$ at $T \ll T_c$ [61]. The *effective* characteristic energy scale $\widetilde{E} = T/f$ then controls all the relevant scales for the geometrical fluctuations and in the two previous limits, it is fixed either by thermal fluctuations ($\widetilde{E} \approx T$) or by disorder ($\widetilde{E} \approx T_c$). From our numerical findings $B_{\rm dis}(r)$ has two power-law regimes with a single crossover lengthscale r_0:

$$B_{\rm dis}(r) = \begin{cases} A_1 (r/r_0)^{2\zeta_{\rm dis}} : & r \ll r_0 \,, \\ A_2 (r/r_0)^{4/3} : & r \gg r_0 \,. \end{cases} \tag{5}$$

We can now fix r_0 with a scaling argument similar to the one used in [44] to determine $\{L_c, \xi_{\rm eff}\}$. We rescale the spatial coordinates $(y = b\bar{y}, u = a\bar{u})$ and parameters $\{c = c', D = D_0 D', T = \widetilde{E} T', \xi = a\xi'\}$ while leaving the Boltzmann weight invariant, so that $B(r; c, D, T, \xi) = a^2 B(r/b; c', D', T', \xi')$. To focus on the microscopic interplay of temperature and disorder, we fix the scales $a = \xi$ and $\widetilde{E} = T/f$ (*i.e.* $\{\xi' = 1, T' = f\}$) which implies $D_0 = \frac{(T/f)^3}{c\xi}$ and $b = \frac{c\xi^2}{T/f}$. The short-lengthscale regime where both the disorder correlation length and the effective energy scale $\widetilde{E}$ are equally relevant lies at $r \leq b$, so that we can identify $r_0 = b$. Note that the effective disorder strength $D' = \frac{T_c}{T} f$ crosses over from $D' \approx 1$ at $T \ll T_c$ to $D' \sim T_c/T$ at $T \gg T_c$: the latter case supports a small-disorder perturbative expansion at high temperature, as physically expected.

We can thus make explicit the prefactors for $B_{\rm dis}(r \leq r_0)$ in (5): $A_1 = B_{\rm dis}(r_0) = A_2$ with A_2 fixed from the large scales from $A_2/r_0^{4/3} = \xi_{\rm eff}^2/L_c^{4/3}$. Using $r_0 = \frac{c\xi^2}{T/f}$, we finally get

$$A_{\rm dis}(T) = \frac{B_{\rm dis}(r \leqslant r_0)}{r^{2\zeta_{\rm dis}}} \propto \frac{\xi^2 T_c^2}{(c\xi^2)^{2\zeta_{\rm dis}}} \left(\frac{f}{T}\right)^{2(1-\zeta_{\rm dis})} \tag{6}$$

This relation entails an important property: a value $\zeta_{\rm dis} = \zeta_{\rm dis}^{\rm th} = 1$ would yield a temperature-independent roughness prefactor. On the contrary, a value $\zeta_{\rm dis} \neq 1$, as we find numerically, implies that the prefactor $A_{\rm dis}(T)$ *does* depend on temperature. This is what we report in Fig. 3, thus further supporting the scenario $\zeta_{\rm dis} < 1$.

From the behavior of the interpolating parameter $f \approx 1$ at $T \gg T_c$ and $f \sim T/T_c$ at $T \ll T_c$, Eq. (6) would imply that $A_{\rm dis}(T)$ decreases with increasing T at $T \gg T_c$ and saturates at $T \to 0$. This scenario is at variance with our numerical findings in Fig. 3: as indicated by the dashed line, $A_{\rm dis}(T)$ does indeed present a regime of temperature $\sim T^{-2(1-\zeta_{\rm dis})}$ compatible with (6). However, such power-law behavior is expected to hold at high T and to provide an upper bound to the low-T saturation. The reasons for this discrepancy are unclear at the moment but could stem from: *(i)* numerical prefactors in the estimation of $T_c(\xi)$, so that the regime $T \ll T_c$ would in fact be reached below our temperature range; *(ii)* the discretization along the internal direction y, which could add one lengthscale to take into account in the scaling analysis. A breakdown of the above scaling argument is not to be excluded, but $r_0 = c\xi^2 f/T$ does coincide with a more involved prediction obtained in the KPZ language [62]. This discrepancy, which does not question our main result namely the existence of the novel power-law roughness regime, clearly requires further investigations that are beyond the scope of the present paper.

Let us now turn to the case of very small thermal fluctuations $T \to 0^+$, where the crossover between the thermal and $\zeta_{\rm dis}$ power-law regimes can be further examined, both analytically and numerically. We first emphasize that the crossover lengthscale r_0 is always bounded by the 'Larkin length' L_c:

$$\begin{cases} T \gg T_c : \; r_0 \ll L_c \,, \text{ with } r_0 \sim \frac{c\xi^2}{T}, \, L_c \sim \frac{T^5}{cD^2} \,, \\ T \ll T_c : \; r_0 \lesssim L_c \sim \frac{T_c^5}{cD^2} = \frac{c^{2/3}\xi^{5/3}}{D^{1/3}} \,. \end{cases} \tag{7}$$

At high temperature, the regime $r \lesssim r_0$ where $B_{\rm dis}(r) \sim r^{2\zeta_{\rm dis}}$ has a small extension and is screened by the thermal contribution Tr/c in $B(r)$; hence, as r increases, the total roughness $B(r)$ crosses over directly from the thermal to the random-manifold regime, with a single crossover at the high-T Larkin length L_c such that $B_{\rm th}(L_c) \approx B_{\rm dis}(L_c)$. On the contrary, in the limit $T \to 0^+$ we have $B(t) \approx B_{\rm dis}(r)$, which crosses over from the new power-law regime that we characterized ($\zeta_{\rm dis}$) to the well-studied random-manifold regime ($\zeta_{\rm KPZ}$), and a vanishing thermal regime at $r \leq r_1 \sim T^{1/[1-2(1-\zeta_{\rm dis})]}$ [63]. By studying the lengthscale r_1 (see SM), we find our numerical results to be compatible with a scaling $\zeta_{\rm dis} \approx 0.91$, but not with $\zeta_{\rm dis} = \zeta_{\rm dis}^{\rm th} = 1$.

Physically the characteristic lengthscales $\{L_c, r_0, r_1\}$ and the energy scale $\widetilde{E} = T/f$ are related to the microscopic interplay between temperature and disorder,

from which they stem from. The 'Larkin length' can be deduced from asymptotically large lengthscales, easier to access both analytically and experimentally, hence its crucial role in previous studies [19, 21, 29, 30, 44, 60]. In this paper, we argue instead that it stems as a consequence of short-lengthscale properties, usually hidden below experimental resolution, that one can nevertheless investigate via the excess roughness due to disorder.

The relevance of these results extends well beyond the sole static 1D interfaces, thanks to the exact mapping onto the 1+1 directed polymer (DP) and the KPZ settings [33, 64]. An interface segment can be seen as a polymer having grown along a DP 'time' (our internal direction y). Fixing an extremity of the DP at the origin, we can focus on its endpoint distribution which encodes, at a fixed 'time' r, the geometrical fluctuations of an equilibrated interface at a lengthscale r. The DP free-energy, *i.e.* the logarithm of this distribution, then obeys a KPZ equation with a 'time' r and a spatially-correlated noise V_p (our random potential), with a so-called 'sharp-wedge' initial condition [64]. Its steady-state properties have been studied through non-perturbative functional-renormalization-group [45], but the understanding of the short-DP-'time' regime is incomplete, either through variational or perturbative approaches [29, 30, 32, 43]. The scope of our results can thus be extended as follows. Considering the free-energy two-point correlator, the scale r_0 corresponds to the DP 'time' at which the maximum of this correlator saturates to its steady-state value [30]; the short-lengthscale power-law regime of $B_{\rm dis}(r)$ governed by $\zeta_{\rm dis}$ that we uncovered describes how the DP free-energy (*i.e.* the KPZ field) distribution evolves at short times. This indicates that, to access the KPZ universality at short times, one needs to disentangle the disorder from the thermal fluctuations, and that this seems be done in a scale-invariant regime governed by $\zeta_{\rm dis}$. Finally, since the Burgers equation is derived from the KPZ one, our results translate to the Burgers turbulence [51] where the small-temperature asymptotics corresponds to the inviscid limit and large-scale forcing [46, 50].

In this work, we have found numerical evidences that, hidden under thermal fluctuations of a 1D interface, there exists a scale-invariant regime at short lengthscales governed by an exponent $\zeta_{\rm dis}$. Our numerical analysis allows in addition to show that $\zeta_{\rm dis} < 1$ at variance with the existing analytical estimates for such an exponent $\zeta_{\rm dis}^{\rm th} = 1$. The discrepancy hints towards the non-perturbative nature of the short-lengthscale regime of $B_{\rm dis}(r)$, which thus requires further analytical investigations. In systems where thermal fluctuations are strong enough, the scaling regime described by $\zeta_{\rm dis}$ is hidden under the thermal fluctuations, but when the temperature becomes small or when the disorder correlation length becomes large, the power-law behaviour $B(r) \sim r^{2\zeta_{\rm dis}}$ can be manifest on an experimentally or numerically accessible range. For instance, large roughness exponents were found in a recent modelization [65] of experimental measurements [66] of magnetic circular domains subjected to an AC field. A possible cause can be that the AC field effectively increases the disorder correlation length in the sample, thus unveiling the $B(r) \sim r^{2\zeta_{\rm dis}}$ regime. It is worth investigating the existence of such scaling regime in interfaces, and to test its robustness to features such as overhangs (for instance in disordered Ginzburg-Landau models [67], known to reduce to qEW in some limit [57]). Adding a driving force generates a small velocity in a non-linear so-called 'creep regime', whose scaling is controlled by the static geometrical exponents. It is natural to wonder if the scaling regime we unveiled has consequence for the creep regime, for instance in avalanches statistics. The case of higher dimensions random manifolds is also open.

Such situation would thus prove a natural direction in which to try to observe this regime in the current experimental implementations of domain walls, such as the magnetic of ferroelectric ones. Such observations, although challenging due to the difficulty to access the small lengthscales would however also provide informations on the stability of this regime to the deviations from the elastic theory.

We thank Jean-Pierre Eckmann and Sebastian Bustingorry for discussions related to this work. This work was supported in part by the Swiss National Science Foundation under Division II. N.C. acknowledges support from the Federal Commission for Scholarships for Foreign Students for the Swiss Government Excellence Scholarship (ESKAS No. 2018.0636). E.A. acknowledges support from the Swiss National Science Foundation by the SNSF Ambizione Grant PZ00P2_173962. V.L. thanks the Université de Genève (where part of this work was performed) for its warm hospitality, and acknowledges support by the ERC Starting Grant No. 680275 MALIG, the ANR-18-CE30-0028-01 Grant LABS and the ANR-15-CE40-0020-03 Grant LSD.

The simulations were performed at the University of Geneva on the *Mafalda* cluster of GPUs.

* Corresponding author: Nirvana.Caballero@unige.ch

[1] D. S. Fisher, Phys. Rep. **301**, 113 (1998).
[2] S. Lemerle, J. Ferré, C. Chappert, V. Mathet, T. Giamarchi, and P. Le Doussal, Phys. Rev. Lett. **80**, 849 (1998).
[3] J. Ferré, P. J. Metaxas, A. Mougin, J.-P. Jamet, J. Gorchon, and V. Jeudy, Comptes Rendus Physique **14**, 651 (2013).
[4] P. Paruch and J. Guyonnet, Comptes Rendus Physique **14**, 667 (2013).
[5] G. Durin, F. Bohn, M. A. Corrêa, R. L. Sommer, P. Le Doussal, and K. J. Wiese, Phys. Rev. Lett. **117**,

087201 (2016).
[6] N. B. Caballero, I. F. Aguirre, L. J. Albornoz, A. B. Kolton, J. C. Rojas-Sánchez, S. Collin, J. M. George, R. D. Pardo, V. Jeudy, S. Bustingorry, and J. Curiale, Phys. Rev. B **96**, 224422 (2017).
[7] R. Diaz Pardo, W. Savero Torres, A. B. Kolton, S. Bustingorry, and V. Jeudy, Phys. Rev. B **95**, 184434 (2017).
[8] E. K. H. Salje, D. Xue, X. Ding, K. A. Dahmen, and J. F. Scott, Phys. Rev. Materials **3**, 014415 (2019).
[9] P. Tückmantel, I. Gaponenko, N. Caballero, J. C. Agar, L. W. Martin, T. Giamarchi, and P. Paruch, Phys. Rev. Lett. **126**, 117601 (2021).
[10] M. Alava, M. Dube, and M. Rost, Advances in Physics **53**, 83 (2004).
[11] S. Santucci, K. J. Måløy, A. Delaplace, J. Mathiesen, A. Hansen, J. Ø. Haavig Bakke, J. Schmittbuhl, L. Vanel, and P. Ray, Phys. Rev. E **75**, 016104 (2007).
[12] L. Laurson, X. Illa, S. Santucci, K. T. Tallakstad, K. J. Måløy, and M. J. Alava, Nature Communications **4**, 1 (2013).
[13] S. Santucci, K. T. Tallakstad, L. Angheluta, L. Laurson, R. Toussaint, and K. J. Måløy, Philosophical Transactions of the Royal Society A **377**, 20170394 (2019).
[14] O. Chepizhko, C. Giampietro, E. Mastrapasqua, M. Nourazar, M. Ascagni, M. Sugni, U. Fascio, L. Leggio, C. Malinverno, G. Scita, S. Santucci, M. J. Alava, S. Zapperi, and C. A. M. La Porta, Proceedings of the National Academy of Sciences **113**, 11408 (2016).
[15] R. Alert and X. Trepat, Annual Review of Condensed Matter Physics **11**, 77 (2020).
[16] G. Rapin*, N. Caballero*, I. Gaponenko, B. Ziegler, A. Rawleight, E. Moriggi, T. Giamarchi, S. A. Brown, and P. Paruch, Scientific Reports **11**, 1 (2021).
[17] L. Berthier and G. Biroli, Rev. Mod. Phys. **83**, 587 (2011).
[18] D. S. Fisher, Phys. Rev. B **31**, 1396 (1985).
[19] G. Blatter, M. V. Feigel'man, V. B. Geshkenbein, A. I. Larkin, and V. M. Vinokur, Rev. Mod. Phys. **66**, 1125 (1994).
[20] P. Chauve, T. Giamarchi, and P. Le Doussal, Europhys. Lett. **44**, 110 (1998).
[21] P. Chauve, T. Giamarchi, and P. Le Doussal, Phys. Rev. B **62**, 6241 (2000).
[22] E. Agoritsas, V. Lecomte, and T. Giamarchi, Physica B **407**, 1725 (2012).
[23] K. J. Wiese, Theory and experiments for disordered elastic manifolds, depinning, avalanches, and sandpiles, arXiv:2102.01215 [cond-mat.dis-nn] (2021).
[24] E. E. Ferrero, L. Foini, T. Giamarchi, A. B. Kolton, and A. Rosso, Annual Review of Condensed Matter Physics **12**, 111 (2021).
[25] A.-L. Barabási and H. E. Stanley, *Fractal Concepts in Surface Growth*, Cambridge University Press ed. (Cambridge, 1995).
[26] D. Jordán, L. J. Albornoz, J. Gorchon, C. H. Lambert, S. Salahuddin, J. Bokor, J. Curiale, and S. Bustingorry, Phys. Rev. B **101**, 184431 (2020).
[27] M. J. Cortés Burgos, P. C. Guruciaga, D. Jordán, C. P. Quinteros, E. Agoritsas, J. Curiale, M. Granada, and S. Bustingorry, Phys. Rev. B **104**, 144202 (2021).
[28] G. Rapin, S. Ehrensperger, C. Blaser, N. Caballero, and P. Paruch, Applied Physics Letters **In press** (2021).
[29] E. Agoritsas, V. Lecomte, and T. Giamarchi, Phys. Rev. B **82**, 184207 (2010).
[30] E. Agoritsas, V. Lecomte, and T. Giamarchi, Phys. Rev. E **87**, 042406 (2013).
[31] E. Agoritsas, V. Lecomte, and T. Giamarchi, Phys. Rev. E **87**, 062405 (2013).
[32] S. E. Korshunov, V. B. Geshkenbein, and G. Blatter, Journal of Experimental and Theoretical Physics **117**, 570 (2013).
[33] M. Kardar, G. Parisi, and Y.-C. Zhang, Phys. Rev. Lett. **56**, 889 (1986).
[34] D. A. Huse, C. L. Henley, and D. S. Fisher, Phys. Rev. Lett. **55**, 2924 (1985).
[35] I. Corwin, Random Matrices: Theory and Applications **01**, 1130001 (2012).
[36] P. Calabrese and P. Le Doussal, Phys. Rev. Lett. **106**, 250603 (2011).
[37] P. L. Doussal and P. Calabrese, J. Stat. Mech. **2012**, P06001 (2012).
[38] T. Halpin-Healy and K. A. Takeuchi, Journal of Statistical Physics **160**, 794 (2015).
[39] J. Quastel and H. Spohn, Journal of Statistical Physics **160**, 965 (2015).
[40] J. P. Bouchaud, M. Mézard, and G. Parisi, Phys. Rev. E **52**, 3656 (1995).
[41] S. E. Korshunov and V. S. Dotsenko, J. Phys. A: Math. Gen. **31**, 2591 (1998).
[42] E. Agoritsas, S. Bustingorry, V. Lecomte, G. Schehr, and T. Giamarchi, Phys. Rev. E **86**, 031144 (2012).
[43] V. Dotsenko, J. Stat. Mech.: Th. Exp. **2016**, 123304 (2016).
[44] E. Agoritsas and V. Lecomte, J. Phys. A: Math. Theor. **50**, 104001 (2017).
[45] S. Mathey, E. Agoritsas, T. Kloss, V. Lecomte, and L. Canet, Phys. Rev. E **95**, 032117 (2017).
[46] V. Dotsenko, J. Stat. Mech.: Th. Exp. **2018**, 083302 (2018).
[47] K. A. Takeuchi, M. Sano, T. Sasamoto, and H. Spohn, Scientific Reports **1**, 34 (2011).
[48] K. A. Takeuchi and M. Sano, Journal of Statistical Physics **147**, 853 (2012).
[49] K. A. Takeuchi, Physica A **504**, 77 (2018).
[50] T. Gotoh and R. H. Kraichnan, Physics of Fluids **10**, 2859 (1998).
[51] J. Bec and K. Khanin, Physics Reports **447**, 1 (2007).
[52] S. F. Edwards and D. R. Wilkinson, Proceedings of the Royal Society A **381**, 17 (1982).
[53] A. B. Kolton, A. Rosso, and T. Giamarchi, Phys. Rev. Lett. **94**, 047002 (2005).
[54] E. E. Ferrero, S. Bustingorry, A. B. Kolton, and A. Rosso, Comptes Rendus Physique **14**, 641 (2013).
[55] E. E. Ferrero, S. Bustingorry, and A. B. Kolton, Phys. Rev. E **87**, 032122 (2013).
[56] J. K. Salmon, M. A. Moraes, R. O. Dror, and D. E. Shaw, in *Proceedings of 2011 International Conference for High Performance Computing, Networking, Storage and Analysis* (2011) pp. 1–12.
[57] N. Caballero, E. Agoritsas, V. Lecomte, and T. Giamarchi, Phys. Rev. B **102**, 104204 (2020).
[58] See Eq. (20) in [32] for the second-order correction at finite temperature, leading to the conjecture stated in Eq. (21).
[59] See Eqs. (56), (126) in [29].
[60] A. I. Larkin, Sov. Phys. JETP **31**, 784 (1970).
[61] See Eqs. (49), (97) in [30].

[62] See Eq. (99) in [30], where the DP 'time' $t_{\rm sat}$ identifies with r_0.
[63] At low T, $B_{\rm th}(r)$ intersects $B_{\rm dis}(r)$ at a crossover $r_1 < r_0$. We can evaluate r_1 at $T \ll T_c$ from $Tr_1/c \equiv A_1(r_1/r_0)^{2\zeta_{\rm dis}}$, which yields $r_1^{1-2(1-\zeta_{\rm dis})} = \frac{T\,(T/f)^{4/3}}{c\xi^{4/3}D^{2/3}} r_0^{2(1-\zeta_{\rm dis})}$ with $T/f \sim T_c$.
[64] D. A. Huse and C. L. Henley, Phys. Rev. Lett. **54**, 2708 (1985).
[65] N. Caballero, J. Stat. Mech. **2021**, 103207 (2021).
[66] P. Domenichini, C. P. Quinteros, M. Granada, S. Collin, J.-M. George, J. Curiale, S. Bustingorry, M. G. Capeluto, and G. Pasquini, Phys. Rev. B **99**, 214401 (2019).
[67] N. B. Caballero, E. E. Ferrero, A. B. Kolton, J. Curiale, V. Jeudy, and S. Bustingorry, Phys. Rev. E **97**, 062122 (2018).

Supporting material for "Microscopic interplay of temperature and disorder of a 1D elastic interface"

Pinning force correlator and disorder strength

In this section, we detail how we generate the quenched random potential $V_p(y,u)$ and its associated pinning force $F_p(y,u) \equiv -\partial_u V_p(y,u)$. We recall that the interface is parametrized by the univalued displacement field $u(y,t)$, with the internal coordinate y taking discrete values $y = j\Delta y$ (where j is an integer, $j = 0, \dots L_y/\Delta y$), and the transverse coordinate u taking continuous values. We consider a disorder with Gaussian distribution fully characterized by a zero mean and the two-point correlators:

$$\begin{aligned} \overline{V_p(y_1,u_1)V_p(y_2,u_2)} &= D\, R_\xi(u_2-u_1)\,\delta_{y_2 y_1}\,, \\ \overline{F_p(y_1,u_1)F_p(y_2,u_2)} &= \Delta_\xi(u_2-u_1)\,\delta_{y_2 y_1}\,, \end{aligned} \tag{8}$$

where $\overline{\cdots}$ denotes the average over disorder realizations. We chose the normalization $\int_{\mathbb{R}} \mathrm{d}u\, R_\xi(u) = 1$, and the correlators are simply related by $\Delta_\xi(u) = -D R''_\xi(u)$. In the following, we thus make explicit the functional $\Delta_\xi(u)$ and the disorder strength D.

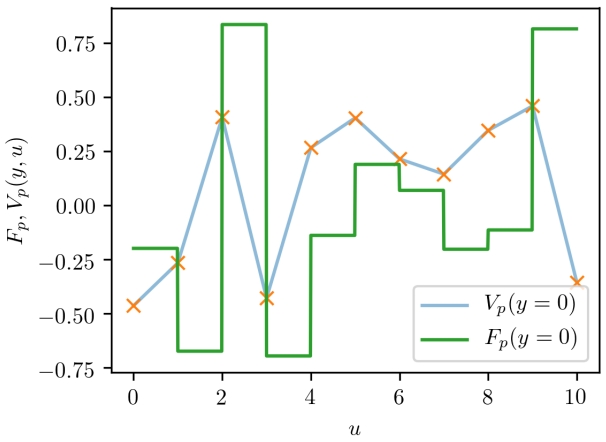

Figure 4. For a fixed coordinate y, the random potential $V_p(y,u)$ is generated by a linear interpolation between random numbers taken from a uniform distribution with zero mean (orange crosses). The associated pinning force F_p is obtained from the associated piecewise derivative $F_p(y,u) = -\partial_u V_p(y,u)$.

Generating a spatially-correlated disorder

The pinning potential $V_p(y,u)$ is defined independently for each discrete value of the coordinate y, so that in what follows, one fixes y and considers only the coordinate u. The procedure to generate the corresponding quenched 'landscape' $U(u) \equiv V_p(y,u)$ at fixed y, spatially-correlated with a finite correlation length ξ, is the following (see Fig. 4). We first discretize the direction u with fixed steps $\Delta u = \xi$. A random number U_k is generated independently at each site $u = k\Delta u$ (with k an integer) from a probability distribution function $\mathcal{P}(U_k)$ of zero mean.

Then, on every interval $u \in [k\Delta u, (k+1)\Delta u]$ (*i.e.* one has $k = \lfloor u/\Delta u \rfloor$) the random pinning potential is defined as a linear interpolation between U_k and U_{k+1}:

$$U(u) = U_k + \frac{U_{k+1}-U_k}{\Delta u}(u - k\Delta u)\,. \tag{9}$$

One can easily check that, as required, this definition satisfies $U(k\Delta u) = U_k$ and $U((k+1)\Delta u) = U_{k+1}$. The associated pinning force $F_p(u) = -\partial_u U(u)$ is finally given by the discrete derivative

$$F_p(u) = -\frac{U_{k+1}-U_k}{\Delta u} \tag{10}$$

with $k = \lfloor u/\Delta u \rfloor$ as above.

For our simulations we sort each reference value U_k from a *uniform* distribution on the interval $[-\frac{\epsilon}{2}, \frac{\epsilon}{2}]$, with $\epsilon > 0$. It has consequently a zero mean and a variance

$$D_0 \equiv \overline{(U_k)^2} = \frac{\epsilon^2}{12}\,. \tag{11}$$

To keep the discussion general, thereafter we generically denote the variance of U_k as a control parameter D_0. In addition, we discuss in Sec. how choosing an alternative distribution $\mathcal{P}(U_k)$ (non-uniform but with the same variance) leads to physically consistent results.

Piecewise linear force correlator

We start by defining the intermediate two-point correlator of the force as

$$\Delta^{(2)}_\xi(u_1,u_2) = \overline{F_p(u_1)F_p(u_2)}\,. \tag{12}$$

Because it is associated to the specific set of intervals $u \in [k\Delta u, (k+1)\Delta u]$ with $k = \lfloor u/\Delta u \rfloor$, it is important to notice that it is *not* invariant by translation along the u direction. Indeed, pairs of points (u_1,u_2) separated by a same distance $u = u_2 - u_1$ can either lie in the same interval $[k\Delta u, (k+1)\Delta u]$ or not.

One has in fact three possibilities: if (u_1,u_2) are

- in the same interval, one has

$$\Delta^{(2)}_\xi(u_1,u_2) = 2\overline{(U_i)^2} = \frac{2D_0}{\Delta u^2}\,; \tag{13}$$

- in adjacent intervals $[(k-1)\Delta u, k\Delta u]$ and $[k\Delta u, (k+1)\Delta u]$:

$$\Delta_\xi^{(2)}(u_1,u_2) = -\overline{(U_i)^2} = -\frac{D_0}{\Delta u^2}\,; \tag{14}$$

- in more distant intervals $[k\Delta u, (k+1)\Delta u]$ and $[j\Delta u, (j+1)\Delta u]$ with $|k-j| \leq 2$:

$$\Delta_\xi^{(2)}(u_1,u_2) = 0\,. \tag{15}$$

And from now on we use that $\xi = \Delta u$ to emphasize the explicit dependence on the correlation length ξ.

To recover a translation-invariant correlator, as required in the definitions (8), one must average the intermediate correlator $\Delta_\xi^{(2)}(u_1,u_2)$ over all pairs of points (u_1,u_2) separated by the same distance u:

$$\Delta_\xi(u) = \int_{\mathbb{R}^2} \mathrm{d}u_1 \mathrm{d}u_2\, \delta(u_2-u_1-u)\, \Delta_\xi^{(2)}(u_1,u_2)\,. \tag{16}$$

One finds by an explicit computation

$$\Delta_\xi(u) = \frac{D_0}{\xi^2}\,\Delta_{\mathrm{adim}}\big(u/\xi\big) \tag{17}$$

with $\Delta_{\mathrm{adim}}(\hat{u})$ the piecewise linear continuous function that connects the values:

$$\Delta_{\mathrm{adim}}(\hat{u}) = 2 \quad \text{for} \quad \hat{u} = 0\,, \tag{18}$$
$$\Delta_{\mathrm{adim}}(\hat{u}) = -1 \quad \text{for} \quad |\hat{u}| = 1\,, \tag{19}$$
$$\Delta_{\mathrm{adim}}(\hat{u}) = 0 \quad \text{for} \quad |\hat{u}| \geq 2\,. \tag{20}$$

The complete function is plotted in the inset of Fig. 5.

As a self-consistent validation of our procedure, we evaluated numerically the correlator $\Delta_\xi(u)$, and as shown in Fig. 5 we find an excellent agreement with the expression (17).

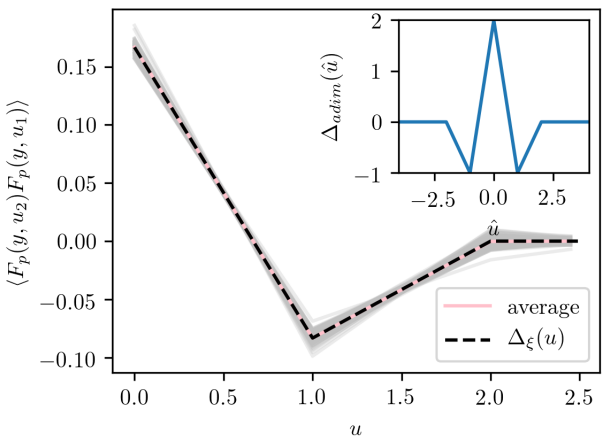

Figure 5. Numerical evaluation of the pinning force correlator for 100 different disorder realizations with $\epsilon = 1$ (gray lines) and its average (pink). In black dashed line we show $\Delta_\xi(u)$, the expected correlator given by Eq. (17) with $D_0 = 1/12$. In the inset, we show the adimensionalized force correlator $\Delta_{\mathrm{adim}}(\hat{u})$ connecting the values of Eqs. (18)-(20).

Correlators in Fourier space and disorder strength

One can check that $\int_{\mathbb{R}} \mathrm{d}\hat{u}\, \Delta_{\mathrm{adim}}(\hat{u}) = 0$, as expected for the 'random-bond' disorder we consider. To access the disorder strength D, we switch to Fourier space where we can more easily exploit the relation between the correlators $\Delta_\xi(u) = -DR''_\xi(u)$ from Eq. (8).

We first rewrite, similarly to Eq. (17), the random potential correlator in terms of its adimensionalized version, starting from its very definition

$$\overline{U(u)U(0)} \equiv DR_\xi(u) \equiv \frac{D}{\xi} R_{\mathrm{adim}}(u/\xi)\,. \tag{21}$$

First, by direct comparison with the definition in Eq. (11) we can establish its relation to the variance D_0:

$$D_0 \equiv \overline{U(0)^2} = DR_\xi(u=0) = \frac{D}{\xi} R_{\mathrm{adim}}(\hat{u}=0)\,, \tag{22}$$

and secondly the relation between the correlators $\Delta_\xi(u) = -DR''_\xi(u)$ becomes

$$\frac{D_0}{\xi^2}\Delta_{\mathrm{adim}}(\hat{u}) = -\frac{D}{\xi^3} R''_{\mathrm{adim}}(\hat{u})\,. \tag{23}$$

Defining the Fourier transform along the transverse direction as $\hat{\Delta}_{\mathrm{adim}}(\hat{q}) = \int_{\mathbb{R}} \mathrm{d}\hat{u}\, e^{i\hat{q}\hat{u}} \Delta_{\mathrm{adim}}(\hat{u})$, one finds by direct computation that it takes the simple form:

$$\hat{\Delta}_{\mathrm{adim}}(\hat{q}) = 16 \frac{\big[\sin\frac{\hat{q}}{2}\big]^4}{\hat{q}^2}\,. \tag{24}$$

Defining similarly the Fourier transform $\hat{R}_{\mathrm{adim}}(\hat{q}) = \int_{\mathbb{R}} \mathrm{d}\hat{u}\, e^{i\hat{q}\hat{u}} R_{\mathrm{adim}}(\hat{u})$, Eq. (23) rewrites

$$\hat{\Delta}_{\mathrm{adim}}(\hat{q}) = \frac{D}{D_0\xi}\hat{q}^2 \hat{R}_{\mathrm{adim}}(\hat{q})\,. \tag{25}$$

At this point, we might think that we have some freedom to define $\hat{R}_{\mathrm{adim}}$ up to an arbitrary constant, but we have in fact to enforce the imposed normalization $\int_{\mathbb{R}} \mathrm{d}u\, R_{\mathrm{adim}}(\hat{u}) = 1$ or equivalently $\hat{R}_{\mathrm{adim}}(\hat{q}=0) = 1$. This is achieved by imposing $\frac{D}{D_0\xi} = 1$ and thus

$$\hat{R}_{\mathrm{adim}}(\hat{q}) = 16\frac{\big[\sin\frac{\hat{q}}{2}\big]^4}{\hat{q}^4} \quad \Rightarrow \quad \lim_{\hat{q}\to 0} \hat{R}_{\mathrm{adim}}(\hat{q}) = 1\,. \tag{26}$$

Furthermore, we have by inverse Fourier transform:

$$R_{\mathrm{adim}}(\hat{u}=0) = \int_{\mathbb{R}} \frac{\mathrm{d}\hat{q}}{2\pi}\, \hat{R}_{\mathrm{adim}}(\hat{q}) = \frac{2}{3}\,. \tag{27}$$

We have, at last, directly access to the disorder strength:

$$D \overset{(22)}{=} \frac{D_0\xi}{R_{\mathrm{adim}}(\hat{u}=0)} \overset{(27)}{=} \frac{3}{2} D_0\xi\,. \tag{28}$$

The last expression is valid for any random potential generated by a linear interpolation between uncorrelated random points, drawn from an arbitrary distribution $\mathcal{P}(U_k)$ with zero mean and variance D_0. For the uniform distribution we consider, Eq. (11) implies

$$D^{\text{uniform}} = \frac{3}{2} D_0 \xi = \frac{1}{8} \epsilon^2 \,. \tag{29}$$

Parameters of numerical simulations

To solve the quenched Edwards-Wilkinson equation (Eq. (1) of the main text) and compute the interface roughness, we take advantage of massively parallel accelerated computing with a CUDA C++ code running in NVIDIA GPUs with a Volta architecture, in double precision. At each simulation step we approximate the second derivative of u along the y-direction by a two-point central finite difference scheme and integrate in time with a first-order Euler step. Pseudo-random numbers are generated with a counter-based RNG (Philox, allowing 2^{64} parallel and distinct streams with a period of 2^{128} [56]). For the thermal noise, we use Gaussian distributed numbers while for the quenched disorder, we use the method described in Sec. (and in Sec. in the consistency check described in the same section): the method consists in a linear interpolation of uniformly distributed random numbers with the implementation proposed in [55]. These random numbers, uncorrelated from site to site, are dynamically generated along the evolution of the interface, *i.e.* we build the disorder at larger u only if the interface has locally wandered further away.

Space discretization along the y-direction is set to 1 and time discretization to 10^{-2}. We can simulate 4 realizations of systems of 512 sites for 10^8 steps in approximately 8 hours. These scheme and parameters give roughness functions in the clean case which are in very good agreement with the theoretical prediction (Eq. (4) in the main text). The corresponding roughness of the simulated systems differs from the theoretically predicted values in less than 10^{-4} for $r \leq 50$ and less than 10^{-3} for larger values of r (both, simulated and predicted roughness functions are shown in Fig. 1 in the main text). This excellent agreement is a strong consistency check that provides a good support for the validity of the numerical procedure in the disordered case.

Disorder generated from a Gaussian distribution

For the temperature $T = 0.01$, we determined the excess roughness $B_{\text{dis}}^{\text{Gauss}}(r)$ for a disorder potential where the U_i's are distributed with a Gaussian distribution with the same variance $\overline{(U_i)^2} = 1/12$ as the uniform one, see Eq. (11). On Fig. 6, $B_{\text{dis}}^{\text{Gauss}}(r)$ is compared to

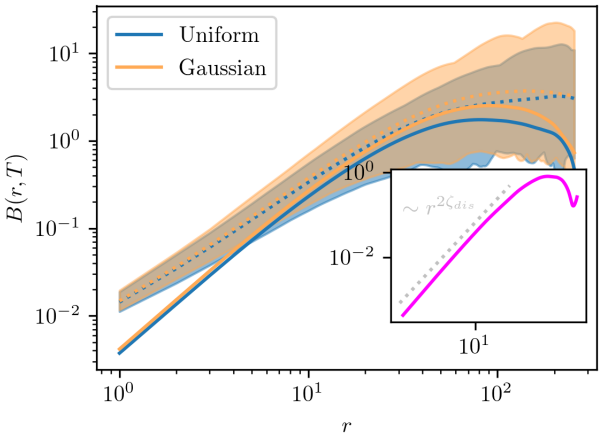

Figure 6. Roughness (dotted lines) and excess roughness (continuous lines) at $T = 0.01$ averaged over 50 realizations with increased statistics, obtained for disorders generated from a uniform and a Gaussian distribution. In the inset we show the difference between both excess roughness.

the excess roughness $B_{\text{dis}}(r)$ computed –as in the rest of the paper– for a disordered potential with the U_i's drawn from a uniform distribution, as described in section .

The results show that $B_{\text{dis}}^{\text{Gauss}}(r)$ is very close to $B_{\text{dis}}(r)$. This provides a strong evidence supporting the following points: in the asymptotic regime $r \to 0$, the power-law behaviour $B_{\text{dis}}(r) \sim r^{2\zeta_{\text{dis}}}$ is universal, *i.e.* presents an exponent ζ_{dis} which does not depend on the specific random-potential disorder distribution. This is an important aspect, as the asymptotic regime $r \to 0$ where $B_{\text{dis}}(r)$ presents the power-law behaviour $\sim r^{2\zeta_{\text{dis}}}$ could have been sensitive to the details of the disorder correlator at small scales. Also, the prefactor A in $B_{\text{dis}}(r) \sim A\, r^{2\zeta_{\text{dis}}}$ is mainly governed by the variance D_0 of the disorder distribution (which is the same in the uniform and in the Gaussian distribution we have used for $\mathcal{P}(u)$). Last, we expect also that this prefactor A depends, through a numerical constant, on the rescaled shape $\Delta_{\text{adim}}(\hat{u})$ of the disorder correlator. This is seen in the small difference $|B_{\text{dis}}^{\text{Gauss}}(r) - B_{\text{dis}}(r)| \ll B_{\text{dis}}(r)$ shown in the inset of Fig. 6. Such difference also scales as $r^{2\zeta_{\text{dis}}}$ in the asymptotic regime $r \to 0$, indicating that indeed only the prefactor A is affected by the adimensionalized shape of the disorder correlator.

Scaling of the crossover scale $r_1(T)$

The crossover scale r_1 is determined numerically by the intersection between the two power-law scalings $B_{\text{dis}}(r) \sim r^{2\zeta_{\text{dis}}}$ and the thermal regime Tr/c. The scaling arguments presented in the main text indicate that

r_1 scales with temperature as

$$r_1(T) \sim \begin{cases} T^{1/[1-2(1-\zeta_{\rm dis})]} & \text{for } T \ll T_c\,, \\ T^5 & \text{for } T \gg T_c\,. \end{cases} \qquad (30)$$

To determine how our numerical results are compatible with such predictions, we have used a fitting function

$$r_1^{\rm fit}(T) = C\,T^{\alpha_-}\left[1 + (T/T^\star)^{\alpha_+ - \alpha_-}\right] \qquad (31)$$

(where C and $T^\star$ are constants and $\alpha_- < \alpha_+$) that interpolates between the regimes $r_1^{\rm fit}(T) \sim T^{\alpha_-}$ for $T \ll T^\star$ and $r_1^{\rm fit}(T) \sim T^{\alpha_+}$ for $T \gg T^\star$. The prediction of Eq. (30) corresponds to

$$\alpha_+ = 5\,, \quad \alpha_- = 1/[1-2(1-\zeta_{\rm dis})]\,. \qquad (32)$$

A first scenario where $\zeta_{\rm dis} = \zeta_{\rm dis}^{\rm th} = 1$ (according to the perturbative analysis of [32], for instance) corresponds to $\alpha_- = 1$. A second scenario where $\zeta_{\rm dis} \approx 0.9 < 1$ corresponds to $\alpha_- \approx 1.25 > 1$. To distinguish between these two possibilities, we have fitted the values of $r_1(T)$ obtained numerically with the function (31), where we fixed the exponent $\alpha_\pm$ and we left the constants C and $T^\star$ as free parameters. As shown on Fig. 7, the data provide a strong evidence supporting the second scenario $\zeta_{\rm dis} \approx 0.9 < 1$. Also, leaving α_- as a free parameter for the fit, one finds $\alpha_- \approx 1.33$ which corresponds to the value $\zeta_{\rm dis} \approx 0.88$: it is compatible with the value $\zeta_{\rm dis} \approx 0.91$ obtained in the main text with a completely different method.

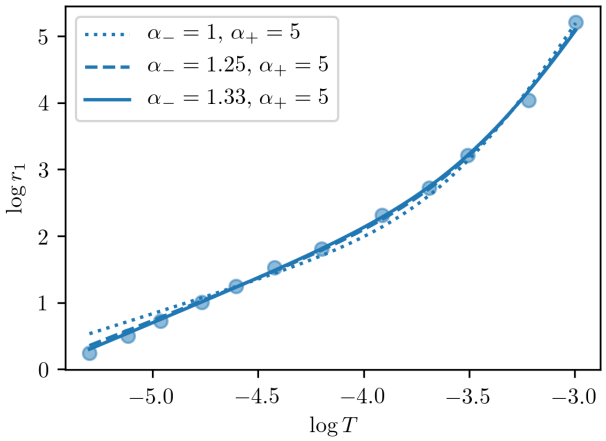

Figure 7. Behaviour of the crossover scale $r_1(T)$. The points are the result of numerical simulations, while the dashed and full line curves correspond to the two scenarios discussed in the text. The exponent $\alpha_- \approx 1.25 > 1$ is more compatible with the numerical data, and corresponds to $\zeta_{\rm dis} \approx 0.9 < 1$.

Determination of the best value of $\zeta_{\rm dis}$

To obtain $\zeta_{\rm dis}$ from the numerical data presented in the main text, we fit $B_{\rm dis}(r,T)$ independently for each value of T in the range $r = [1, r_f]$. For the nine lowest temperatures we have studied, we find values of $\zeta_{\rm dis}$ between 0.9 and 0.92. To determine the best value of this exponent that is compatible with every temperature we considered, we rely on the following scaling argument. We predict that $B_{\rm dis}(r_0,T)/r_0^{2\zeta_{\rm dis}}$ should be independent of r_0 for all temperatures T. In Fig. 8, we illustrate that the best choice of $\zeta_{\rm dis}$ that ensures this collapse is $\zeta_{\rm dis} = 0.91 \pm 0.01$. We quantify the spread of the functions $B_{\rm dis}(r,T)/r^{2\zeta_{\rm test}}$ around their mean value for different values of $\zeta_{\rm test}$ by computing the function $F_{T,r}(\zeta) = \Sigma_{T,r}\left(\frac{B_{\rm dis}(r,T)/r^{2\zeta} - \Sigma_{r_i} B_{\rm dis}(r_i,T)/r_i^{2\zeta}}{\Sigma_{r_i} B_{\rm dis}(r_i,T)/r_i^{2\zeta}}\right)^2$ with $r_i = 1, \ldots, 5$, for the 5 lowest studied temperatures. The resulting function has a minimum in $\zeta = 0.91$, as shown in the inset of Fig. 8.

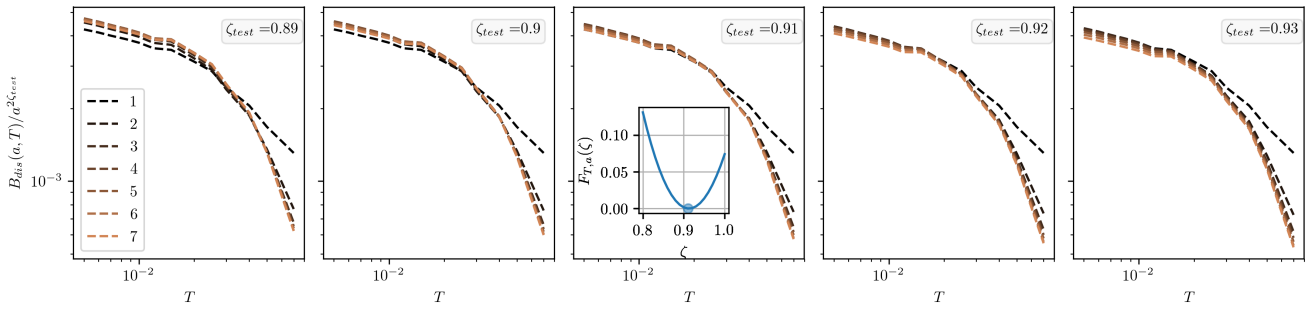

Figure 8. Numerical collapse of the excess roughness, described in the text, for values ζ_{test} of ζ_{dis} ranging from 0.89 to 0.93. The value achieving the best collapse is $\zeta_{\text{dis}} = 0.91$. At 0.91 the function $F_{T,a}(\zeta)$ (see text) has a minimum, as shown in the inset. The different dashed lines correspond to the value of a indicated in the caption.